RSC Advances

PAPER

View Article Online
View Journal | View Issue

Cite this: *RSC Adv.*, 2018, **8**, 17132

Synthesis and photoluminescence properties of Eu^{3+}-activated $LiCa_3ZnV_3O_{12}$ white-emitting phosphors

Xiaoyong Huang * and Heng Guo

Single-component white-emitting phosphors are highly promising for applications in phosphor-converted white light-emitting diodes. In this paper, novel single-phase $LiCa_{3(1-x)}ZnV_3O_{12}:Eu^{3+}$ (x = 0–0.05) phosphors with tunable white emissions were prepared by a conventional solid-state reaction. The $LiCa_3ZnV_3O_{12}$ (x = 0) phosphor showed an efficient self-activated bluish-green emission due to the V^{5+}–O^{2-} charge transfer transition of the $[VO_4]^{3-}$ groups, and possessed an intense broad excitation spectrum in the 250–400 nm wavelength range. Together with the $[VO_4]^{3-}$ emission, the red emission of Eu^{3+} ions was also observed in $LiCa_{3(1-x)}ZnV_3O_{12}:Eu^{3+}$ phosphors. The energy transfer from the $[VO_4]^{3-}$ groups to the Eu^{3+} ions was studied. Importantly, the emission colors of $LiCa_{3(1-x)}ZnV_3O_{12}:Eu^{3+}$ phosphors varied from greenish-blue to whitish and then to red with increasing Eu^{3+} content and the white-light emission was realized in the single-phase phosphor of $LiCa_3ZnV_3O_{12}$:0.003Eu^{3+} by combining the $[VO_4]^{3-}$-emission and the Eu^{3+}-emission. The energy-transfer efficiency from $[VO_4]^{3-}$ groups to Eu^{3+} ions in the $LiCa_3ZnV_3O_{12}$:0.003Eu^{3+} sample was determined to be about 52% and the internal quantum efficiency of the $LiCa_3ZnV_3O_{12}$:0.003Eu^{3+} phosphor was found to be about 41.5%. In addition, the CIE chromaticity coordinates of $LiCa_3ZnV_3O_{12}$:0.003Eu^{3+} were (x = 0.3374, y = 0.3596), and the correlated color temperature was estimated to be about 5311 K.

Received 10th April 2018
Accepted 4th May 2018

DOI: 10.1039/c8ra03075h

rsc.li/rsc-advances

1. Introduction

Solid-state lighting based on white light-emitting diodes (WLEDs) is considered as a next-generation lighting source for general illumination because it offers some particularly intriguing advantages over conventional lighting sources, including outstanding energy efficiency, long working lifetime, eco-friendliness, small size, and fast response time.[1–10] To realize pure white emissions for WLEDs, a common strategy at present is coating phosphors onto the surface of LED chips. Such so-called phosphor-converted WLEDs are generally fabricated through three approaches: (1) combining a blue LED chip with a yellow phosphor (*e.g.*, YAG:Ce^{3+}) or a blend of green and red phosphors, (2) combining an ultraviolet (UV) LED chip with a blend of tricolor (blue, green, and red) phosphors, and (3) combining an UV LED chip with a single-phased white-emitting phosphor.[11–14] Nowadays, the widely used WLEDs are fabricated by coating YAG:Ce^{3+} yellow phosphors on InGaN blue LED chips, however these WLEDs commonly suffer from high correlated color temperature (CCT) and low color rendering index (CRI) owing to the lack of a red component, limiting their applications in indoor lighting.[15–21] On the other hand, the WLEDs made by multiple-emitting phosphors also have some drawbacks, such as intrinsic color balance, device complication and high cost.[22–28] Compared to former two approaches, the latest approach is highly promising, due to its high luminescence efficiency, color repeatability, and low manufacturing costs.[29–31] Therefore, it is urgent to develop high-efficiency single-component white-light-emitting materials.

A powerful way to realize tunable white emissions from single host materials is to control the energy transfer from the sensitizers to the activators.[32] Based on the principle of energy transfer, various single-component white-emitting phosphors were developed recently. However, these white-emitting phosphors are usually fabricated with multiple dopants including Ce^{3+}–Mn^{2+},[33] Eu^{2+}–Mn^{2+},[34] Ce^{3+}–Tb^{3+}–Mn^{2+},[24] and Eu^{2+}–Tb^{3+}–Mn^{2+},[35,36] which require complicate sample-preparation procedures (such as reducing atmosphere) and thus result in significant increase in cost. In sharp contrast, so far there are still few reports on single-activator-doped white-emitting phosphors. In 2007, Li and Lin reported white emission from $CaIn_2O_4$:1.0%Eu^{3+} phosphors due to the $^5D_{0,1,2,3} \rightarrow {}^7F_J$ (J = 0, 1, 2, 3, 4) transitions, but its internal quantum efficiency (IQE) was very low (only 10%).[37] In 2011, Shi and co-workers demonstrated white emission in $K_2YZr(PO_4)_3$:-Eu^{3+} phosphors by combining the Zr^{4+} greenish-blue emission and the Eu^{3+} red emission, while the value of IQE was not given.[38] In 2013, Qian *et al.* reported white light-emitting Y_2WO_6:Sm^{3+} phosphor with low IQE of 21.65%, and the white emission was

Key Lab of Advanced Transducers and Intelligent Control System, Ministry of Education and Shanxi Province, College of Physics and Optoelectronics, Taiyuan University of Technology, Taiyuan 030024, PR China. E-mail: huangxy04@126.com

achieved by combining the green emission from the host with the orange-red emission from the Sm^{3+} dopant.[39]

Recently, vanadates with the self-activated photoluminescence have gained much attention for potential in near-UV-excited white LEDs, as they possess broad and intense charge transfer (CT) absorption bands in the near-UV wavelength range and can exhibit broadband visible emissions corresponding to the V^{5+}–O^{2-} CT transition.[40–50] Recently, several groups reported white-light emissions from Eu^{3+}-activated vanadate-based phosphors, such as $Sr_{2.91}V_2O_8$:0.06Eu^{3+},[51] and $Sr_2V_2O_7$:Eu^{3+}.[41] However, no value of the IQE was given. Just recently, Hasegawa and co-workers reported the bluish white emission from the $LiCa_3ZnV_3O_{12}$ (abbreviated as: LCZV) host with high IQE.[52] To the best of our knowledge, the luminescence properties of Eu^{3+}-doped LCZV have not been reported in the literature.

In this paper, we reported the synthesis and luminescence properties of a novel high-efficiency single-component white-emitting LCZV:Eu^{3+} phosphor. A series of LCZV:Eu^{3+} phosphors with different Eu^{3+} doping concentrations were prepared by conventional solid-state reaction under air atmosphere (no need the reducing atmosphere). Amazingly, these phosphors have intense broad excitation bands in 250–400 nm range peaking at 343 nm due to the $[VO_4]^{3-}$ groups. Moreover, energy transfer from the LCZV host to Eu^{3+} ions took place. Under 343 nm excitation, LCZV:Eu^{3+} phosphors gave rise to bright tunable white light by combining the broad bluish-green emission band peaking at 500 nm of LCZV host and the red emission lines of Eu^{3+} ions. Importantly, the LCZV:0.003Eu^{3+} white-light-emitting sample showed a high IQE of 41.5% along with CIE chromaticity coordinates of ($x = 0.3374$, $y = 0.3596$) and a CCT = 5311 K.

2. Experimental

$LiCa_{3(1-x)}ZnV_3O_{12}$:xEu^{3+} (x = 0, 0.001, 0.003, 0.005, 0.01, 0.02, and 0.05) powder phosphors were prepared *via* a conventional high-temperature solid-state reaction technique. The raw materials of $CaCO_3$ (analytical reagent, AR), Li_2CO_3 (AR), ZnO (AR), NH_4VO_3 (AR), and Eu_2O_3 (99.99%) were weighed based on stoichiometric ratios and ground in an agate mortar. Subsequently, the obtained mixtures were putted into the alumina crucibles and pre-sintered in a furnace at 750 °C for 6 h in air, and then the obtained powders were re-ground and sintered again at 850 °C for 6 h. The final products were ground into fine powders and used for characterizations.

The X-ray diffraction (XRD) patterns were recorded on a Bruker D8 X-ray diffractometer using Cu Kα radiation. The photoluminescence (PL) and photoluminescence excitation (PLE) spectra were recorded with an Edinburgh FS5 spectrometer equipped with a 150 W continued-wavelength xenon lamp as excitation source. The IQE of the phosphors was measured on an Edinburgh FS5 spectrometer equipped with a barium sulfate-coated integrating sphere.

3. Results and discussion

Fig. 1 presents the representative XRD patterns of LCZV:xEu^{3+} (x = 0.001, 0.005, and 0.05) samples. For the samples doped with low Eu^{3+} concentrations ($x = 0.001$ and 0.005), all the diffraction peaks can be indexed to standard data of $LiCa_3MgV_3O_{12}$ (JCPDS no. 24-1212). However, for the LCZV:0.05Eu^{3+} sample, a small diffraction peak at 24.58° due to the $EuVO_4$ impurity (JCPDS no. 15-0809) was presented. Since the radii of Ca^{2+} (1.12 Å, coordinate number (CN) = 8) and Eu^{3+} ions (1.06 Å, CN = 8) were similar,[45] Eu^{3+} dopants in the LCZV:Eu^{3+} phosphors are likely to replace the Ca^{2+} sites. The LCZV:Eu^{3+} phosphors crystallized into the pure cubic phase with space group $Ia\bar{3}d$.

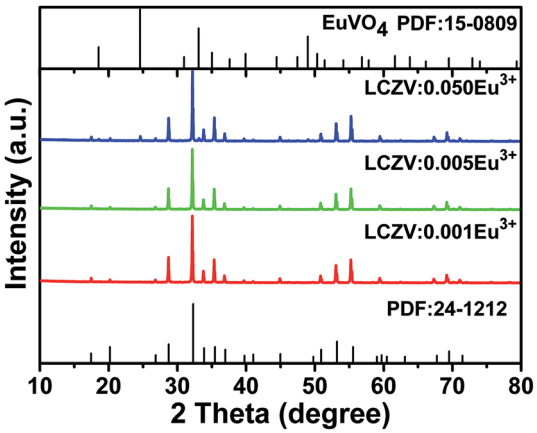

Fig. 1 XRD patterns of LCZV:xEu^{3+} samples.

Fig. 2 shows the diffuse reflectance spectra of LCZV:xEu^{3+} (x = 0 and 0.003) phosphors. It can be seen that for both samples, a strong broad absorption band was presented in the 200–400 nm near-UV wavelength, which was assigned to the ligand to metal CT transition between V^{5+}–O^{2-} in the $[VO_4]$ tetrahedral.[45,52] However, due to the low doping concentration of Eu^{3+} ions, the absorption peaks of Eu^{3+} ions were not observed.[53]

The CLZV host belongs to a self-activated bluish-green emitting phosphor. Fig. 3 presents the PLE and PL spectra of the LCZV host. As shown in Fig. 3(a), the PLE spectrum monitoring at 520 nm exhibited an intense broad band in the 250–400 nm wavelength range with a maximum at 343 nm, which agreed well with the diffuse reflectance spectrum of the LCZV host. Moreover, by using Gaussian fitting, the PLE band

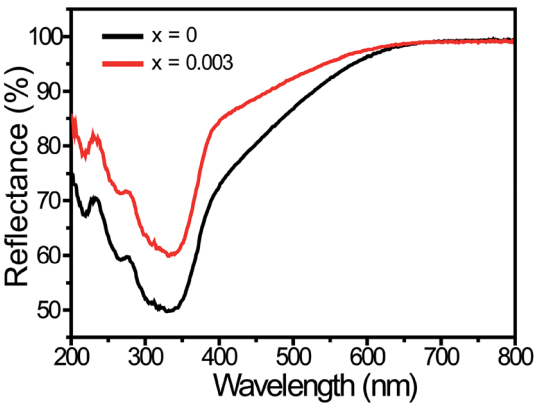

Fig. 2 Diffuse reflectance spectra of the LCZV:xEu^{3+} ($x = 0$ and 0.003) phosphors.

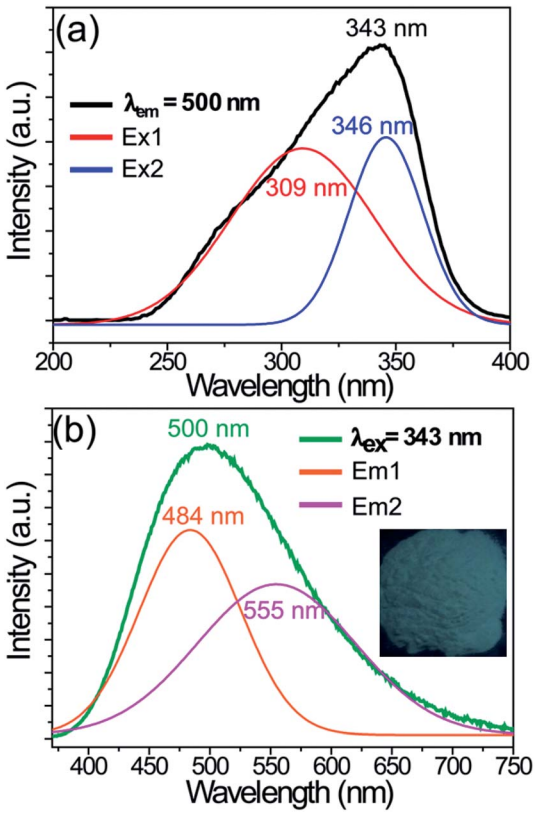

Fig. 3 PLE (a) and PL (b) spectra of the LCZV host material. Inset shows the digital photo of the sample under a 365 nm UV lamp.

consisted of two sub-bands corresponding to the $^1A_1 \rightarrow {}^1T_2$ (Ex1; 309 nm) and $^1A_1 \rightarrow {}^1T_1$ (Ex2; 346 nm) transitions of $[VO_4]^{3-}$ groups.[40,42,52] Upon 343 nm excitation, the CLMV host gave rise to a strong broad bluish-green emission band in the 370–750 nm wavelength region peaking at about 500 nm, as demonstrated in Fig. 3(b). Meanwhile, by using the Gaussian fitting, the PL band was composed of two sub-bands due to $^3T_2 \rightarrow {}^1A_1$ (Em1; 484 nm) and $^3T_1 \rightarrow {}^1A_1$ (Em2; 555 nm) transitions of $[VO_4]^{3-}$ groups.[40,42,52]

Fig. 4 shows the PLE and PL spectra of the LCZV:0.003Eu^{3+} phosphors. The PLE spectrum was monitored at 609 nm corresponding to the $^5D_0 \rightarrow {}^7F_2$ transition of Eu^{3+} ions and it consisted of a strong broad PLE band in the 250–400 nm wavelength range due to V^{5+}–O^{2-} CT transition of $[VO_4]^{3-}$ groups. Besides, a relatively weak sharp PLE peak at 394 nm corresponding to the $^7F_0 \rightarrow {}^5L_6$ transition of Eu^{3+} ions was also presented in the PLE spectrum. These observations indicated that energy transfer from $[VO_4]^{3-}$ groups to Eu^{3+} ions in LCZV:Eu^{3+} phosphors took place. Under 343 nm excitation, the LCZV:0.003Eu^{3+} showed bright white emission, as shown in Fig. 4. The obtained PL spectrum exhibited a broad emission band with a maximum at 500 nm due to the $[VO_4]^{3-}$ groups and several sharp emission lines of Eu^{3+} ions ($^5D_0 \rightarrow {}^7F_1$ transition at 589 nm, $^5D_0 \rightarrow {}^7F_2$ transition at 609 nm, $^5D_0 \rightarrow {}^7F_3$ transition at 652 nm, and $^5D_0 \rightarrow {}^7F_4$ transition at 708 nm).[54–58] The energy transfer efficiency (η_{ET}) of $[VO_4]^{3-} \rightarrow Eu^{3+}$ in LCZV:0.003Eu^{3+} sample can be calculated by using the equation below:[59]

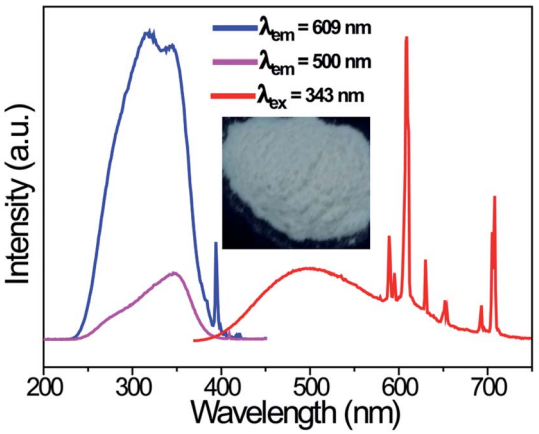

Fig. 4 PLE (λ_{em} = 500 and 609 nm) and PL (λ_{ex} = 343 nm) spectra of the LCZV:0.003Eu^{3+} phosphors. Inset shows the photograph of the sample under a 365 nm UV lamp.

$$\eta_{ET} = 1 - \frac{I}{I_0} \quad (1)$$

where I_0 and I represent the PL intensities of LCZV host and LCZV:0.003Eu^{3+} phosphors, respectively. Then, the η_{ET} was calculated to be about 52%.

Fig. 5 schematically shows the energy transfer process from $[VO_4]^{3-}$ to Eu^{3+} ions in LCZV:Eu^{3+} phosphors. Upon 343 nm UV light excitation into the $[VO_4]^{3-}$ groups, electrons are then excited from the ground state $^1A_1$ into the $^1T_1$ and $^1T_2$ higher-excited levels. Subsequently, the excited electrons at the $^1T_1$ and $^1T_2$ levels relax to the $^3T_2$ and $^3T_1$ lower-excited levels *via* nonradiative relaxation processes and then return to the ground state, thus giving rise to the bluish-green emissions corresponding to the $^3T_2 \rightarrow {}^1A_1$ and $^3T_1 \rightarrow {}^1A_1$ transitions. Once Eu^{3+} ions are doped into LCZV host, partial excited energy of $[VO_4]^{3-}$ groups at the $^3T_1$ level would be transferred to the $^5D_0$ level of

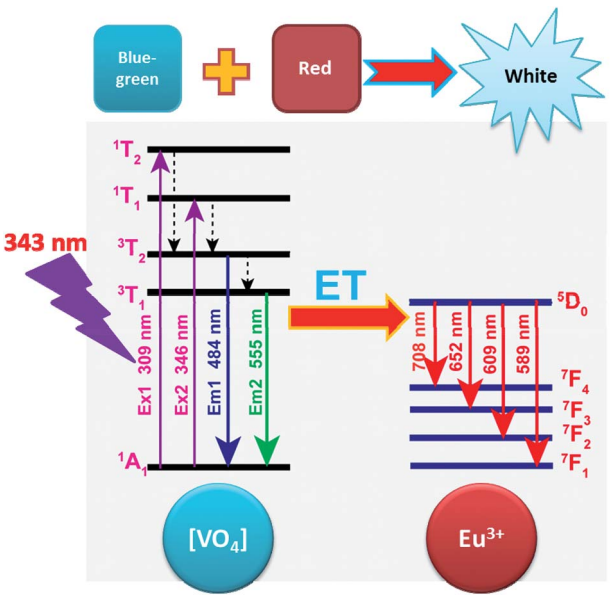

Fig. 5 Energy transfer scheme for the tunable white emissions in LCZV:Eu^{3+} phosphors. ET denotes energy transfer.

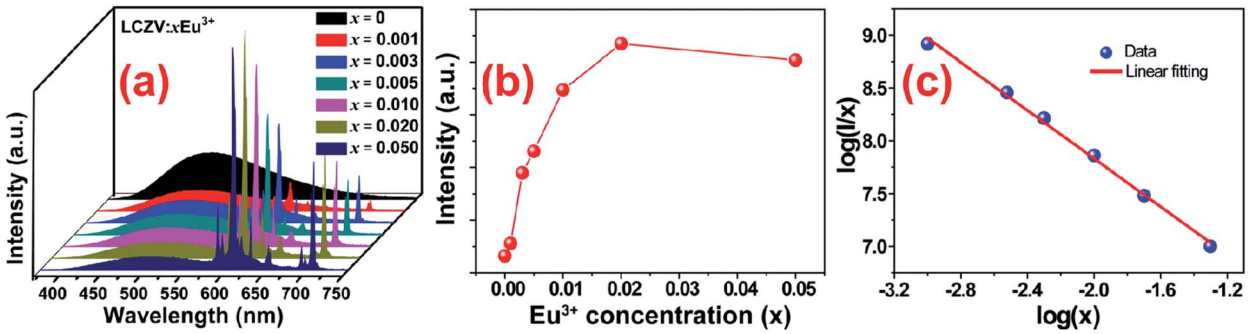

Fig. 6 (a) PL spectra of LCZV:xEu^{3+} (x = 0, 0.001, 0.003, 0.005, 0.01, 0.02, and 0.05) phosphors under 343 nm excitation. (b) The intensity of 609 nm emission as a function of Eu^{3+} concentration in LCZV:xEu^{3+} phosphors. (c) The plot of log(I/x) *vs.* log(x) in LCZV:xEu^{3+} phosphors.

nearby Eu^{3+} ions through the nonradiative resonant process, finally leading to the population of the $^5D_4$ excited levels and subsequently the red emissions due to the $^5D_0 \rightarrow {}^7F_{1,2,3,4}$ transitions. By controlling the Eu^{3+} doping concentration, the energy transfer efficiency from $[VO_4]^{3-}$ to Eu^{3+} ions can be adjusted, and thus intensity ratios of bluish-green and red emissions could be manipulated. Accordingly, tunable white emissions would be achieved.

In order to realize tunable white emissions, a series of Eu^{3+}-activated LCZV phosphors with various Eu^{3+} doping concentrations were prepared. Fig. 6(a) shows the PL spectra of LCZV:xEu^{3+} (x = 0, 0.001, 0.003, 0.005, 0.01, 0.02, and 0.05) phosphors under 343 nm excitation. It can be seen that with increasing Eu^{3+} doping concentrations, the PL intensity of the blue-green emission from LCZV host gradually reduced, further confirming the energy-transfer from LCZV host to Eu^{3+} activators. In contrast, with the increasing Eu^{3+} concentrations in LCZV:xEu^{3+}, the PL emission intensity of Eu^{3+} ions gradually increased first and reached the maximum value at x = 0.02; whereas further increasing the Eu^{3+} doping concentration resulted in reduced intensity of Eu^{3+} red emissions owing to the concentration quenching effect (see Fig. 6(b)). Generally, the occurrence of concentration quenching comes from the energy migration among the activators until energy sink in the host lattice is reached.[60] The probability of energy migration is inversely proportional to R_n, where R is the distance between the activator ions and n is an integer. The critical average distance (R_c) among Eu^{3+} ions in the LCZV host lattice can be roughly calculated by using the following expression:[61]

$$R_c = 2\left(\frac{3V}{4\pi x_c Z}\right)^{1/3} \quad (2)$$

where R_c is the critical distance, V is the volume of the unit cell, x_c is the critical doping concentration, and Z is the number of formula units per unit cell. In this present work, the x_c = 0.02; V = 1926.86 Å^3; and Z = 8.[52] The critical average distance R_c for Eu^{3+} ions in LCZV host material was determined to be about 28.44 Å.

As well-known, nonradiative energy migration among luminescence activators can take place through exchange interaction or multipole–multipole interaction. The exchange interaction only works if the distance between activators is shorter than 5 Å. In our case, the R_c = 28.44 Å, and thus electric multipolar interaction would be the dominant energy transfer mechanism between Eu^{3+} ions in LCZV host. The type of interaction mechanism can be determined by the following equation:[62]

$$\log(I/x) = A - (\theta/3)\log x \quad (3)$$

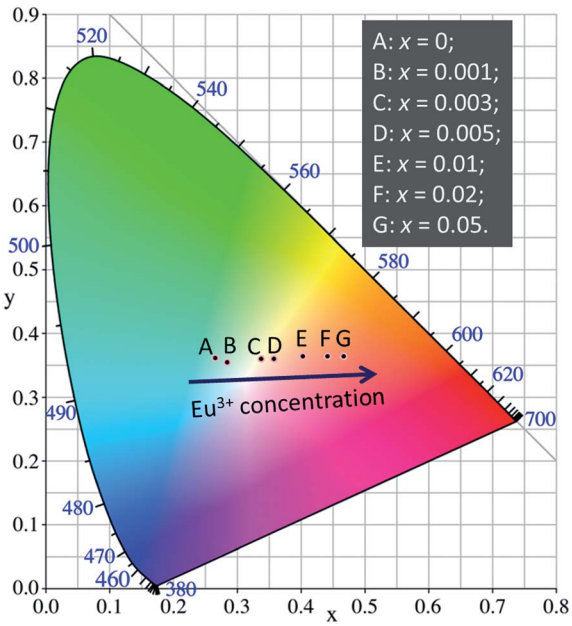

Fig. 7 CIE chromaticity diagram for LCZV:xEu^{3+} phosphors with various doping concentrations of Eu^{3+} ions.

Table 1 CIE chromaticity coordinates and CCTs of LCZV:xEu^{3+} phosphors with different Eu^{3+} doping concentrations

Sample (x)	CIE (x, y)	CCT (K)
0	(0.2648, 0.3608)	8690
0.001	(0.2841, 0.3549)	7749
0.003	(0.3374, 0.3596)	5311
0.005	(0.3570, 0.3601)	4612
0.01	(0.4022, 0.3634)	3345
0.02	(0.4417, 0.3642)	2551
0.05	(0.4673, 0.3639)	2173

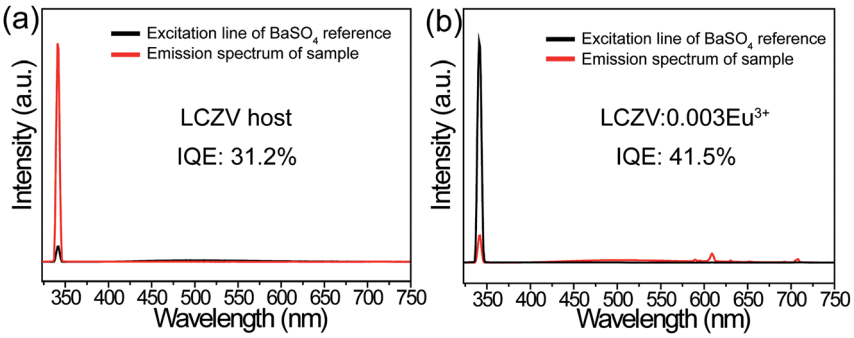

Fig. 8 Excitation line of $BaSO_4$ and the emission spectrum of LCZV host collected using an integrating sphere. (b) Excitation line of $BaSO_4$ and the emission spectrum of LCZV:0.003Eu^{3+} phosphors collected using an integrating sphere.

where I is the PL intensity, x is the dopant concentration, A is concentration, and $\theta = 6$, 8 and 10 refers to dipole–dipole, dipole-quadrupole and quadrupole–quadrupole interactions, respectively. Fig. 6(c) shows the plot of $\log(I/x)$ *vs.* $\log(x)$. The experimental data can be well-fitted into linear line with a slop of −1.14. Accordingly, θ value was calculated to be 3.42, and this value was close to 3. This result indicated that the nonradiative energy transfer among the nearest-neighbor ions was the mechanism of Eu^{3+} concentration quenching effect in LCZV:Eu^{3+} phosphors.[63] Similar results also have been previously reported in Eu^{3+}-activated $Li_3Gd_3Te_2O_{12}$, $Ba_3La(PO_4)_3$, and $Sr_{1.7}Zn_{0.3}CeO_4$ phosphors.[64–66]

The values of CIE chromaticity coordinates of LCZV:$x$$Eu^{3+}$ phosphors were shown in Fig. 7 and Table 1. Obviously, the emission colors of LCZV:$x$$Eu^{3+}$ phosphors can be readily tuned from bluish-green ($x = 0.2648$, $y = 0.3608$) to white ($x = 0.3374$, $y = 0.3596$), and then to red ($x = 0.4673$, $y = 0.3639$) by raising the Eu^{3+} doping concentrations, which can be attributed to the energy transfer from the $[VO_4]^{3-}$ groups to Eu^{3+} ions. Particularly, by controlling the Eu^{3+} doping concentration, white emissions were achieved in single-phased LCZV:$x$$Eu^{3+}$ phosphors through the suitable combination of the $[VO_4]^{3-}$ bluish-green emissions and the Eu^{3+} red emissions. Based on these values of CIE chromaticity coordinates, the CCTs for these tunable emissions were calculated by using the following equation:[67]

$$\mathrm{CCT} = 437n^3 + 3601n^2 - 6861n + 5541.31 \quad (4)$$

where $n = (x - x_c)/(y - y_c)$, and the (x_c, y_c) of chromaticity epicenter is (0.3320, 0.1858). The calculated CCT values were also listed in Table 1. For the LCZV:0.003Eu^{3+} white-emitting phosphors, the CCT was found to be about 5311 K.

As well-known, the IQE is an important factor for evaluating the performance of inorganic luminescent materials. Thus, we have measured the IQEs of LCZV host material and the white-emitting LCZV:0.003Eu^{3+} phosphors (see Fig. 8), and their values were calculated by using the following expression,[68,69]

$$\eta = \frac{\int L_S}{\int E_R - \int E_S} \quad (5)$$

Here η is the IQE, L_S shows the emission spectrum of the studied samples, E_R and E_S present the PLE spectra of the excitation light with and without synthesized compounds, respectively. Accordingly, the IQEs of the LCZV host and white-emitting LCZV:0.003Eu^{3+} phosphors were determined to be about 31.2% and 41.5% under 343 nm excitation. Significantly, the value of the IQE for LCZV:0.003Eu^{3+} sample was much higher than several previous reported white-emitting phosphors, such as $CaIn_2O_4$:Eu^{3+} (IQE: 10%),[37] and Y_2WO_6:Sm^{3+} (IQE: 21.65%).[39] It should be noted that the IQE would be further enhanced by optimizing the synthesis process.

4. Conclusions

In summary, in this work, self-activated LCZV host material and Eu^{3+} singly doped LCZV phosphors were prepared by a high-temperature solid-state reaction and their PL properties were investigated. It was found that the LCZV host was a self-activated phosphor. The PLE spectrum of LCZV host consisted of a broad band in the 250–400 nm range, while its PL spectrum excited at 343 nm included a broad band in the greenish-blue region peaking at 500 nm. Interestingly, doping Eu^{3+} ions into LCZV host induced tunable color emissions from LCZV:Eu^{3+} phosphors *via* raising Eu^{3+} doping concentrations and the white-light emission was realized by combining the $[VO_4]^{3-}$ greenish-blue emission with the Eu^{3+} red emission. The LCZV:0.003Eu^{3+} phosphors emitted bright white light with CIE chromaticity coordinates of ($x = 0.3374$, $y = 0.3596$) and CCT = 5311 K. The energy transfer efficiency from $[VO_4]^{3-}$ groups to Eu^{3+} ions in LCZV:0.003Eu^{3+} phosphors was calculated to be 52%. The IQE of LCZV:0.003Eu^{3+} phosphors was determined to be about 41.5%. Our results demonstrated these single-phased white-emitting phosphors would find potential applications in lighting and display systems.

Conflicts of interest

There are no conflicts to declare.

Acknowledgements

This work was supported by the National Natural Science Foundation of China (no. 51502190), the Program for the Outstanding Innovative Teams of Higher Learning Institutions of Shanxi, and the Open Fund of the State Key Laboratory of

Luminescent Materials and Devices (South China University of Technology, no. 2017-skllmd-01).

References

1 X. Zhang, B. Xu, J. Zhang, Y. Gao, Y. Zheng, K. Wang and X. W. Sun, *Adv. Funct. Mater.*, 2016, **26**, 4595–4600.
2 S. Pimputkar, J. S. Speck, S. P. DenBaars and S. Nakamura, *Nat. Photonics*, 2009, **3**, 180–182.
3 P. Pust, P. J. Schmidt and W. Schnick, *Nat. Mater.*, 2015, **14**, 454.
4 R. Haitz and J. Y. Tsao, *Phys. Status Solidi A*, 2011, **208**, 17–29.
5 X. Li, Y. Liu, X. Song, H. Wang, H. Gu and H. Zeng, *Angew. Chem., Int. Ed.*, 2015, **54**, 1759–1764.
6 X. Huang, B. Li and H. Guo, *J. Alloys Compd.*, 2017, **695**, 2773–2780.
7 X. Huang and H. Guo, *Dyes Pigm.*, 2018, **152**, 36–42.
8 J. Liang, P. Du, H. Guo, L. Sun, B. Li and X. Huang, *Dyes Pigm.*, 2018, **157**, 40–46.
9 J. Han, L. Li, M. Peng, B. Huang, F. Pan, F. Kang, L. Li, J. Wang and B. Lei, *Chem. Mater.*, 2017, **29**, 8412–8424.
10 J. Zhong, D. Chen, Y. Zhou, Z. Wan, M. Ding and Z. Ji, *J. Eur. Ceram. Soc.*, 2016, **36**, 1705–1713.
11 P. Pust, V. Weiler, C. Hecht, A. Tücks, A. S. Wochnik, A.-K. Henß, D. Wiechert, C. Scheu, P. J. Schmidt and W. Schnick, *Nat. Mater.*, 2014, **13**, 891–896.
12 X. Huang, *Nat. Photonics*, 2014, **8**, 748–749.
13 R. Cao, W. Wang, J. Zhang, S. Jiang, Z. Chen, W. Li and X. Yu, *J. Alloys Compd.*, 2017, **704**, 124–130.
14 W. Dai, Y. Lei, J. Zhou, Y. Zhao, Y. Zheng, M. Xu, S. Wang and F. Shen, *J. Am. Ceram. Soc.*, 2017, **100**, 5174–5185.
15 H. Zhu, C. C. Lin, W. Luo, S. Shu, Z. Liu, Y. Liu, J. Kong, E. Ma, Y. Cao, R.-S. Liu and X. Chen, *Nat. Commun.*, 2014, **5**, 4312.
16 S. S. Liang, M. M. Shang, H. Z. Lian, K. Li, Y. Zhang and J. Lin, *J. Mater. Chem. C*, 2016, **4**, 6409–6416.
17 M. Peng, X. Yin, P. A. Tanner, C. Liang, P. Li, Q. Zhang and J. Qiu, *J. Am. Ceram. Soc.*, 2013, **96**, 2870–2876.
18 M. Peng, X. Yin, P. A. Tanner, M. G. Brik and P. Li, *Chem. Mater.*, 2015, **27**, 2938–2945.
19 R. Cao, Y. Ye, Q. Peng, G. Zheng, H. Ao, J. Fu, Y. Guo and B. Guo, *Dyes Pigm.*, 2017, **146**, 14–19.
20 Y.-Y. Zhou, E.-H. Song, T.-T. Deng and Q.-Y. Zhang, *ACS Appl. Mater. Interfaces*, 2018, **10**, 880–889.
21 M. Zhu, Y. Pan, Y. Huang, H. Lian and J. Lin, *J. Mater. Chem. C*, 2018, **6**, 491–499.
22 Y. Jia, R. Pang, H. Li, W. Sun, J. Fu, L. Jiang, S. Zhang, Q. Su, C. Li and R.-S. Liu, *Dalton Trans.*, 2015, **44**, 11399–11407.
23 F. Kang, Y. Zhang and M. Peng, *Inorg. Chem.*, 2015, **54**, 1462–1473.
24 X. Zhang and M. Gong, *Dalton Trans.*, 2014, **43**, 2465–2472.
25 J. Ding, Q. Wu, Y. Li, Q. Long, C. Wang and Y. Wang, *Dalton Trans.*, 2015, **44**, 9630–9636.
26 M. Jiao, Y. Jia, W. Lu, W. Lv, Q. Zhao, B. Shao and H. You, *Dalton Trans.*, 2014, **43**, 3202–3209.
27 Y. Liu, G. Liu, J. Wang, X. Dong and W. Yu, *Inorg. Chem.*, 2014, **53**, 11457–11466.
28 A. Huang, Z. Yang, C. Yu, Z. Chai, J. Qiu and Z. Song, *J. Phys. Chem. C*, 2017, **121**, 5267–5276.
29 Y. Woo Seo, S. Heum Park, S. Hyoung Chang, J. Hyun Jeong, K. Ho Kim and J.-S. Bae, *Ceram. Int.*, 2017, **43**, 8497–8501.
30 M. Jiao, Y. Jia, W. Lu, W. Lv, Q. Zhao, B. Shao and H. You, *J. Mater. Chem. C*, 2014, **2**, 90–97.
31 C. Zhou, Y. Tian, O. Khabou, M. Worku, Y. Zhou, J. Hurley, H. Lin and B. Ma, *ACS Appl. Mater. Interfaces*, 2017, **9**, 40446–40451.
32 K. Li, M. M. Shang, H. Z. Lian and J. Lin, *J. Mater. Chem. C*, 2016, **4**, 5507–5530.
33 G. Li, D. Geng, M. Shang, C. Peng, Z. Cheng and J. Lin, *J. Mater. Chem.*, 2011, **21**, 13334–13344.
34 N. Guo, Y. Huang, M. Yang, Y. Song, Y. Zheng and H. You, *Phys. Chem. Chem. Phys.*, 2011, **13**, 15077–15082.
35 W. Lü, Z. Hao, X. Zhang, Y. Luo, X. Wang and J. Zhang, *Inorg. Chem.*, 2011, **50**, 7846–7851.
36 W.-R. Liu, C.-H. Huang, C.-W. Yeh, Y.-C. Chiu, Y.-T. Yeh and R.-S. Liu, *RSC Adv.*, 2013, **3**, 9023–9028.
37 X. Liu, C. Lin and J. Lin, *Appl. Phys. Lett.*, 2007, **90**, 081904.
38 L. Shi and H. J. Seo, *Opt. Express*, 2011, **19**, 7147–7152.
39 H. Qian, J. Zhang and L. Yin, *RSC Adv.*, 2013, **3**, 9029–9034.
40 T. Nakajima, M. Isobe, T. Tsuchiya, Y. Ueda and T. Manabe, *J. Phys. Chem. C*, 2010, **114**, 5160–5167.
41 W.-Q. Yang, H.-G. Liu, M. Gao, Y. Bai, J.-T. Zhao, X.-D. Xu, B. Wu, W.-C. Zheng, G.-K. Liu and Y. Lin, *Acta Mater.*, 2013, **61**, 5096–5104.
42 J. Zhou, F. Huang, J. Xu, H. Chen and Y. Wang, *J. Materi. Chem. C*, 2015, **3**, 3023–3028.
43 T. Nakajima, M. Isobe, Y. Uzawa and T. Tsuchiya, *J. Materi. Chem. C*, 2015, **3**, 10748–10754.
44 R. Yu, J. H. Jeong and Y.-F. Wang, *J. Am. Ceram. Soc.*, 2017, **100**, 5649–5658.
45 P. Du and J. S. Yu, *Dyes Pigm.*, 2017, **147**, 16–23.
46 X. Y. Huang, J. X. Wang, D. C. Yu, S. Ye, Q. Y. Zhang and X. W. Sun, *J. Appl. Phys.*, 2011, **109**, 113526.
47 R. Cao, D. Peng, H. Xu, Z. Luo, H. Ao, S. Guo and J. Fu, *Optik*, 2016, **127**, 7896–7901.
48 R. Cao, D. Peng, H. Xu, S. Jiang, T. Fu, W. Luo and Z. Luo, *Spectrochim. Acta, Part A*, 2015, **150**, 465–469.
49 F. Kang, H. Zhang, L. Wondraczek, X. Yang, Y. Zhang, D. Y. Lei and M. Peng, *Chem. Mater.*, 2016, **28**, 2692–2703.
50 F. Kang, M. Peng, D. Y. Lei and Q. Zhang, *Chem. Mater.*, 2016, **28**, 7807–7815.
51 S. J. Yoon and K. Park, *Opt. Mater.*, 2014, **36**, 1305–1310.
52 T. Hasegawa, Y. Abe, A. Koizumi, T. Ueda, K. Toda and M. Sato, *Inorg. Chem.*, 2018, **57**, 857–866.
53 X. Zhou, L. Chen, S. Jiang, G. Xiang, L. Li, X. Tang, X. Luo and Y. Pang, *Dyes Pigm.*, 2018, **151**, 219–226.
54 X. Huang, *Dyes Pigm.*, 2016, **130**, 99–105.
55 X. Huang, B. Li, H. Guo and D. Chen, *Dyes Pigm.*, 2017, **143**, 86–94.
56 P. Du, X. Huang and J. S. Yu, *Chem. Eng. J.*, 2018, **337**, 91–100.
57 B. Li and X. Huang, *Ceram. Int.*, 2018, **44**, 4915–4923.
58 X. Huang, S. Wang, B. Li, Q. Sun and H. Guo, *Opt. Lett.*, 2018, **43**, 1307–1310.

59 B. Li, X. Huang, H. Guo and Y. Zeng, *Dyes Pigm.*, 2018, **150**, 67–72.
60 C.-K. Chang and T.-M. Chen, *Appl. Phys. Lett.*, 2007, **91**, 081902.
61 G. Blasse, *Phys. Lett. A*, 1968, **28**, 444–445.
62 D. L. Dexter, *J. Chem. Phys.*, 1953, **21**, 836–850.
63 Q. Shao, H. Ding, L. Yao, J. Xu, C. Liang and J. Jiang, *RSC Adv.*, 2018, **8**, 12035–12042.
64 H. Deng, Z. Gao, N. Xue, J. H. Jeong and R. Yu, *J. Lumin.*, 2017, **192**, 684–689.
65 R. Yu, H. M. Noh, B. K. Moon, B. C. Choi, J. H. Jeong, K. Jang, S. S. Yi and J. K. Jang, *J. Alloys Compd.*, 2013, **576**, 236–241.
66 H. Li, R. Zhao, Y. Jia, W. Sun, J. Fu, L. Jiang, S. Zhang, R. Pang and C. Li, *ACS Appl. Mater. Interfaces*, 2014, **6**, 3163–3169.
67 C. S. McCamy, *Color Res. Appl.*, 1992, **17**, 142–144.
68 X. Huang, B. Li, P. Du, H. Guo, R. Cao, J. S. Yu, K. Wang and X. W. Sun, *Dyes Pigm.*, 2018, **151**, 202–210.
69 H. Guo, X. Huang and Y. Zeng, *J. Alloys Compd.*, 2018, **741**, 300–306.